Neutralization and equilibration of highly charged argon ions at grazing incidence on a graphite surface

S. Winecki, C. L. Cocke, D. Fry,* and M. P. Stöckli
J. R. Macdonald Laboratory, Department of Physics, Kansas State University, Manhattan, Kansas 66506-2604
(Received 26 December 1995; revised manuscript received 15 February 1996)

Final-charge-state distributions of argon ions, scattered grazingly from a smooth highly oriented pyrolytic graphite surface, have been measured as a function of initial charge state ($q=4-17$) and impact velocity ($v=0.15-0.62$ a.u.) The final-charge-state distribution changes strongly with the impact velocity, but is almost independent of the initial charge state. The neutralization during grazing-angle scattering is compared to the charge-state equilibration experienced by ions passing through a solid (carbon foil), and these two processes seem to have common properties. A K x-ray spectrum from the K-shell vacancy decay of 51-KeV Ar^{17+} projectiles was obtained as a function of the angle between the ion beam and the surface. Measurements of x-ray spectra in coincidence with grazingly scattered ions are reported. A simple model for argon neutralization near and below the surface is proposed. The model assumes a direct side feeding into the Ar M shell followed by Auger and radiative L- and K-shell filling. [S1050-2947(96)09806-X]

PACS number(s): 34.50.Dy

I. INTRODUCTION

The neutralization of ions during an interaction with solids and solid surfaces has attracted substantial attention and has been studied both theoretically and experimentally for many years. Particularly, the neutralization of highly charged ions that carry multiple inner-shell vacancies remains to a large extent not understood. An updated review of this subject can be found in the article by Burgdörfer [1]. The experimental observations show that the highly charged ion interacting with the solid experiences a rapid neutralization and relaxation [2–4]. The following physical ''picture'' of the ion-solid interaction has been adopted. The highly charged ion captures electrons from the solid at a relatively large distance from the surface via a resonant charge transfer. Because of an energy matching, the capture populates highly excited states and a hollow atom is formed. This initial stage of the ion-surface interaction seems to be well described by an over-barrier model [1,5]. The hollow atom undergoes deexcitation via Auger or radiative decay that populates lower states. The deexcitation rates are, however, generally too small to allow a full relaxation of the ion before it hits the surface. This is particularly true because the image charge force that accelerates the ion towards the surface sets the lower limit for the time the hollow atom can spend above the surface. The hollow atom hits the surface and ejects its loosely bounded electrons either into the bulk or outside the solid (peeloff process) [4,6]. Therefore, it is commonly argued that the resonant capture into high states and the Auger (radiative) decays that follow are not sufficient to explain the high degree of neutralization and relaxation seen in the experiment. To explain the neutralization an additional mechanism is introduced and is usually referred to as a side feeding [7]. The side feeding is believed to take place at a smaller distance from the surface and to populate lower ionic states than the resonant charge exchange. In addition, the electron exchange rate associated with the side feeding is assumed to be large in order to account for the rapid and complete neutralization observed experimentally. It should be noted that, beyond these postulates, the side-feeding mechanism is still a matter of discussion. Several models describing the side feeding at the surface and inside the solid have been developed in recent years. The over-barrier model worked out by Burgdörfer *et al.* [1,4,5] has been successful in describing side-feeding neutralization above the surface. Another example is the molecular-orbital model by Stolterfoht *et al.* [8] that describes the neutralization inside the solid.

Another aspect of the neutralization of highly charged ions during their interaction with surfaces which is not fully understood is the role of inner-shell vacancies, particularly the vacancies with large binding energies. The possibility that deeply bound inner-shell vacancies are filled by the side-feeding mechanism is questionable, because of large energy differences between these vacancies and the band structure of the solid. This is particularly the case during the interaction of heavy ions with light target solids ($Z_{ion}>Z_{solid}$), where the binding energy of the inner-shell solid electrons is much smaller than the binding energy of inner-shell vacancies of the ion. Under such conditions only Auger or x-ray decay would be expected to be responsible for the inner-shell vacancy filling. However, it has not been quantitatively demonstrated that the transition rates are sufficiently fast to explain the full relaxation of the ion. Partially, this occurs because most of the experimental work in this field has been done with heavy metallic targets and light ions ($Z_{ion}<Z_{solid}$) for which the direct side feeding into inner-shell vacancies seems quite possible. This complicates the interpretation of the experimental data.

The neutralization of highly charged ions at the surface or inside the solid can be studied using several experimental techniques [2–14]. The two commonly used ones are detection of final charge states after grazing-angle reflection from the surface and x-ray spectroscopy. In particular, several ex-

*Present address: Cyclotron Institute, Texas A&M University, College Station, TX 77843.

periments motivated our work. The final charge distributions of argon ions, following the grazing-angle reflection from the gold target were investigated by Meyer *et al.* [2]. Initial charge states between $q=2$ and 14 were used and it was found that the final-charge-state distributions were almost identical for all initial charge states, which means that the L-shell vacancies are efficiently filled during the collision. However, the mechanism for this filling is not clear because the possibility of side feeding into the L shell of argon cannot be excluded from the gold target (many energy levels). Meyer *et al.* used relatively low-velocity ions (0.22 a.u.) and the question arises what will happen at larger velocities. Common intuition might suggest that as the collision time becomes shorter, full relaxation of the ion will not be completed and the influence of the initial charge state might become more pronounced. Another question not investigated by Meyer *et al.* for Ar ions is the mechanism for filling of K-shell vacancies. The very large K-shell binding energy of hydrogenlike argon ($\sim$4.5 keV), suggests that the side feeding of the K-shell vacancy might be much more difficult that of the L-shell vacancies due to the large mismatch between projectile and target energy levels. In our work we address above questions by using a large range of impact velocities and argon ions with charge states up to $q=17$ (one K-shell vacancy). The target used in our experiment, graphite, has a simple electronic structure; even the most tightly bounded K-shell electrons in carbon are not in resonance with the K and L shells of the Ar^{17+} projectiles, and this should strongly inhibit side feeding into the K or L shell of the projectile.

X-ray spectroscopy has been previously employed by several groups [9–14] to investigate the decay of K-shell vacancies present in Ar^{17+} projectiles during collisions with different surfaces. Usually these experiments have determined the x-ray spectrum for different impact angles, from normal incidence down to very small angles of the order of 1°. In the work of Schultz *et al.* [12] angles from 60° to 3° were examined. The high-resolution measurement by d'Etat *et al.* [13] examined angles between 45° and 2°. The critical angle for nonpenetrating trajectories [1], for these two experiments, can be estimated as $\sim$6° [12] and $\sim$4° [13]. This means that the lowest incident angles examined in both experiments involved reflected trajectories. However, in both experiments, the observed x-ray spectra were interpreted as a sum of two components, one emitted above the surface and second emitted after bulk penetration. We believe that this interpretation is not correct for small-angle collisions. There is no below-surface component to the x-ray emission, because the projectiles are reflected from the surface. In the present work the x-ray spectra involving small impact angles were obtained in a different manner. Instead of detection of all x rays, only the x rays in coincidence with the reflected ions were used. This ensures that all ions that for any reason are not reflected at the surface are excluded. The spectra for bigger impact angles were obtained without the coincidence requirement.

In the theoretical part of this work we present a simple model for the neutralization and the relaxation of Ar^{17+} ions at the surface and inside of the solid. The model was motivated by the recent experiment by Briand *et al.* [14], who demonstrated that during the collision of $Ar^{16,17+}$ ions with a SiH surface the L and K shells of argon are fed by Auger or x-ray transitions. The model used in this work assumes that the side feeding populates the M shell of argon. In addition, we assume that one mechanism is responsible for the side feeding inside the solid and at the surface. We will demonstrate that such an assumption is strongly supported by our experimental data. The charge-exchange rate associated with the side feeding is modeled by using fitting parameters. The filling of L and K shells is realized through the Auger and the x-ray decays only without side feeding. As it will be demonstrated, the model correctly describes the properties of x-ray spectra for different impact angles and is consistent with the full neutralization of Ar^{17+} ions.

II. EXPERIMENT

A. Experimental setup

The experiment was performed using the Kansas State University Electron Beam Ion Source (EBIS) [15,16]. Argon ions were used with charge states from $q=4$ up to $q=17$. The source is located on a high-voltage platform which allowed us to explore velocities between 0.15 and 0.62 a.u. The ion beam was highly collimated by two sets of four jaw slits, such that the size of the beam in the interaction region was approximately 0.2 mm full-width at half-maximum (FWHM) and the angular divergence was approximately 0.1° (FWHM) for all used charge states and energies. The highly oriented pyrolytic graphite (HOPG) was used as a target with a well known surface structure C(0001) [17–20]. The azimuthal orientations of the crystallites are randomly distributed [21]. The extremely low surface absorption coefficient [22] and an absence of oxidation layer ensures cleanliness. The layered structure of graphite simplified the preparation of an atomically flat and UHV compatible surface, which was done by removing several top layers with adhesive tape and placing the sample immediately in the vacuum. This procedure has been previously used, and has proved to produce a sufficiently high-quality surface for grazing-angle experiments [23,24]. The whole experiment was performed under UHV conditions, with a typical pressure in a target region of 8×10^{-10} Torr.

The scattering geometry is schematically shown in Fig. 1. During the scattering, ions experience a reflection in a plane normal to the surface as well as an angular spread in a direction parallel to this plane. A post-target set of slits was used to allow a charge-state separation of the reflected ions. A relatively narrow slice of the reflected beam was charge-state separated by an electrostatic deflector. A two-dimensional position-sensitive microchannel-plate detector was located downstream of the deflector. Such an experimental arrangement allowed simultaneous measurement of angular distributions and charge-state distributions of the reflected ions. An identical geometry was used previously [2–4]. A solid state Si(Li) x-ray detector was used to detect K_α and K_β lines emitted by Ar^{17+} projectiles. The detector was located in front of the surface so x rays emitted in a direction normal to the ion beam was detected. The solid angle of the detector was 0.19 sr and its resolution was 220 eV at 5.9keV. The energy calibration of the Si(Li) detector was obtained by using a K x-ray emission from magnesium source and a K x-ray fluorescence from chlorine.

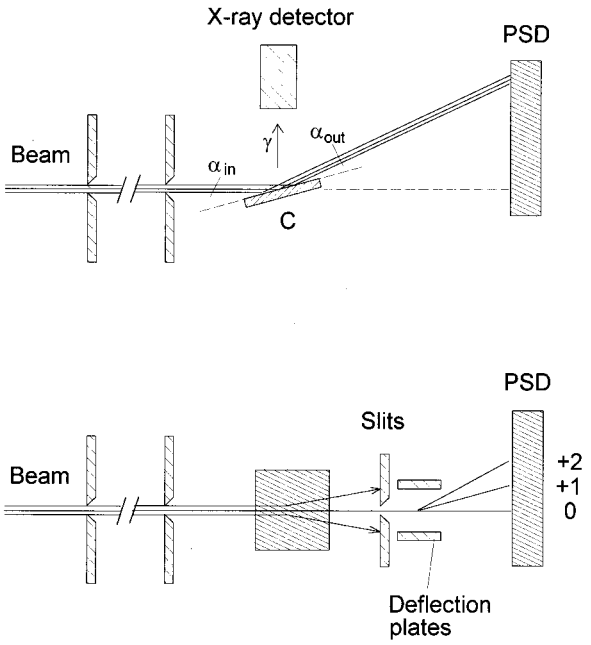

FIG. 1. Side and top views of the experimental setup.

B. Surface quality

The quality of the surface is a key component in any surface scattering experiment. Particularly, grazing-angle geometry is vulnerable to surface defects and contamination. A reliable interpretation of experimental results can be accomplished only if an atomically flat and clean surface is used. On the other hand, it is unrealistic to expect that the surface is defect-free; for example, atomic steps are unavoidable. As it was mentioned above, the layered structure of HOPG allows an easy way to prepare UHV clean surface. The layered structure may, however, cause some surface imperfections, such as deviation from the flatness or local disintegration of an interlayer bonding (defoliation). In order to ensure that the quality of the surface used in our work does not falsify our results, various tests were performed. The graphite surface was observed by an atomic force microscope, which confirmed that about 80% of the total surface was free from defoliation and relatively flat. Typical (local) angular deviation from the perfectly flat surface was not more than 0.1°, which is consistent with the mosaicity of 0.4° (FWHM) for the entire sample quoted by the manufacturer. We have identified large atomically flat areas and atomic size steps between them. These steps were ~ 6 Å in height, which corresponds to a double spacing between the layers in graphite and is consistent with previous work [25]. Some single-layer steps were also observed. The density of steps was relatively small, a typical picture (40 μm$\times$40 μm in size) containing approximately 500 μm (total length) of steps. Using this number and a scattering angle of 1.6°, we estimate that only $\sim 0.3\%$ of ions are scattered or absorbed by atomic size steps. A more serious threat to the quality of the reflection was the local defoliation of the graphite layers, perhaps caused by the removal of top layers and a stress applied to the surface during this operation. Such defoliation was visible on approximately 10–20% of the surface and around edges of the sample. The typical angular deviation from the normal direction for these parts of the surface was approximately 0.5°–1°. These areas, together with small number of macroscopic size steps, were expected to absorb ions, or cause large-angle scattering. In addition, the small size of the target (12×12 mm^2) made it difficult to achieve a perfect overlap between an effective target width and the ion beam.

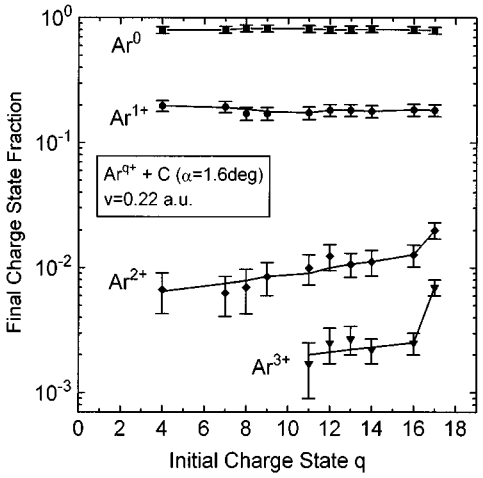

FIG. 2. Final projectile charge fractions for 51-keV Ar^{q+} ($q=4-17$) ions incident on a graphite surface at 1.6°. The lines have been drawn to guide the eye.

A combination of above effects created the possibility that some of the ions were not grazingly reflected from the surface. In order to test this we have measured the fraction of ions reflected from the surface. The graphite target was uniformly moved into the ion beam and the number of reflected ions, as well as the number of ions in the ion beam, were recorded as a function of the target position. The ions were detected by the large (40-mm diam) detector placed ~ 140 mm behind the target. This arrangement assured that nearly all of the reflected ions were detected. The reflection coefficient was found to be 40–70 % and was dependent on the divergence of the beam and the part of the target bombarded. The charge state or velocity of the ion did not have a measurable influence on the reflection coefficient. In addition, we confirmed that vacuum conditions were not a critical factor. The fraction of reflected ions was unchanged even after increasing the pressure in the target region by three orders of magnitude ($\sim 10^{-7}$ Torr). These findings suggest that the ions which were not reflected were absorbed by target imperfections or were not in overlap with the target. We believe that these effects do not influence our experimental results, since all of our grazing-angle measurements involved detection of the reflected ions. That part of the experiment at larger impact angles is not expected to be significantly affected by the surface defects.

III. RESULTS AND DISCUSSION

A. Final-charge-state distribution following grazing-angle collisions

A first part of the experiment was focused on the final-charge-state distributions as a function of the initial charge state and the velocity of the ion. The final-charge-state distribution as a function of initial charge state for an energy of 51 keV is shown in Fig. 2. The data clearly show that an introduction of L-shell vacancies, or even one K-shell va-

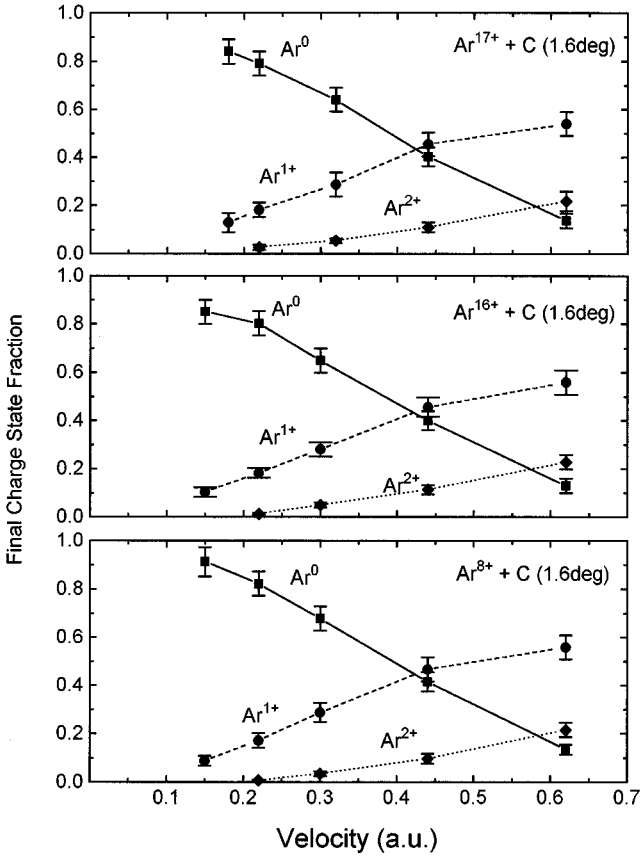

FIG. 3. Velocity dependence of final projectile charge fractions for Ar^{8+}, Ar^{16+}, and Ar^{17+} ions incident on a graphite surface at 1.6°. The lines have been drawn to guide the eye.

cancy, into the system has only a minor influence on the final charge state. A small effect can be noticed for the high final charge states ($q=2$ and larger). However, these channels account only for 1–3 % of the total number of reflected ions, and the average final charge state does not change significantly. These findings mean that the carbon target, with its energetically localized electronic structure, neutralizes argon ions in a way similar to that observed by Meyer *et al.* [2] for a gold target. Because the side feeding into L or K shells of the argon from the carbon target is unlikely, the Auger and the radiative decays must be sufficient to allow a full decay of the inner vacancies.

The velocity dependence of the final-charge-state distribution for three initial charge states, Ar^{8+}, Ar^{16+}, and Ar^{17+}, is shown in Fig. 3. This choice of initial charge states probes the influence of initial inner-shell vacancies, as an Ar^{8+} projectile has an empty M shell but full inner shells, an Ar^{16+} projectile has empty M and L shells, but full K shell, and finally an Ar^{17+} has a one K-shell vacancy. Figure 3 clearly shows that all the initial charge states have, within the experimental error, the same velocity dependence. Therefore, all collision time does not seem to affect the recombination of the inner vacancies.

The velocity dependence in Fig. 3 is quite strong. The average final charge state significantly increases with increasing velocity, from 0.1 at $v=0.15$ a.u. to 1.3 at the highest investigated velocity of 0.62 a.u. The data suggest that

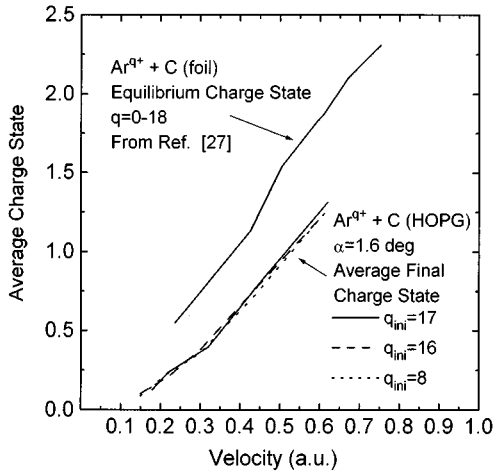

FIG. 4. Average final argon projectile charge states for grazing-angle scattering (this work) and the equilibrium charge states for argon passing through a carbon foil [26]. The lines are drawn to guide the eye.

even at the highest velocity of 0.62 a.u. the collision time is sufficiently long for the total decay of all inner vacancies. This excludes Auger decay as the possible cause of the increased final charge states at the higher velocities. The velocity dependence shown in Fig. 3 must be explained by the presence of electron-loss process which increases with velocity.

Figure 4 compares the final average charge state for grazing collisions with the average equilibrium charge state [26] for argon ions passing through a carbon foil (experimental values) [27]. The foils yield an average charge state which is approximately 0.5 higher than that from surfaces, but exhibit the same velocity dependence. This similarity strongly indicates that the neutralization during grazing-angle scattering from the surface is very similar to the neutralization inside the solid. Furthermore, it indicates that the neutralization rate and the electron-loss rate are similar for the two cases.

B. *K* x-ray emission from Ar^{17+} projectiles

As was shown above, L- and K-shell vacancy relaxation is completed during grazing-angle scattering from the range of velocities investigated here. In a second part of our experiment we have focused on the possible mechanism for this relaxation, using Ar^{17+} projectiles. The Ar^{17+} ion has almost all electrons missing and its full decay should take longer than the decay of any lower-charge-state projectile. The velocity of 0.22 a.u. was used because Fig. 4 suggests that electron loss can be neglected at this low velocity. X-ray spectra for impact angles below 3° were measured in coincidence with projectiles reflected from the surface. In this case the spectrum contamination due to random coincidences was negligible, in order of 1 event per 1000. The spectra for larger impact angles were obtained without the coincidence requirement. A typical coincidence x-ray spectrum, obtained at a grazing angle of 1.3°, is shown in Fig. 5. The spectrum consists of two peaks due to $K\alpha$ and $K\beta$ transitions in argon. These lines were fitted with two Gaussians to determine their mean energies which are presented as a function of impact

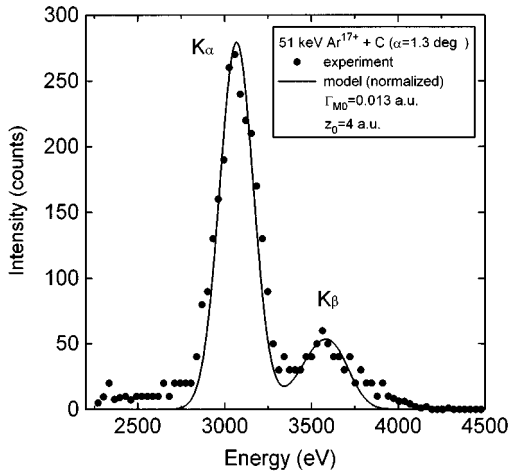

FIG. 5. A typical x-ray spectrum from Ar^{17+} in coincidence with ions grazingly reflected by a graphite surface. The theoretical curve is from the model described in the text. The absolute intensity of theoretical spectrum was normalized to fit the size of the experimental $K\alpha$ peak.

angle in Fig. 6. The energy of both lines shifts upwards for the low impact angles, as has been seen in previous experiments. The absolute value of energy is in agreement with the results by Schultz *et al.* [12]. This experiment was chosen for comparison because the ion energy was exactly the same as in our work. It is worth noting that the experiment by Schultz *et al.* used a germanium instead of graphite target, but this change seems to have no effect on the x-ray spectrum. Our coincidence measurements are in agreement with noncoincidence data from Schultz *et al.*

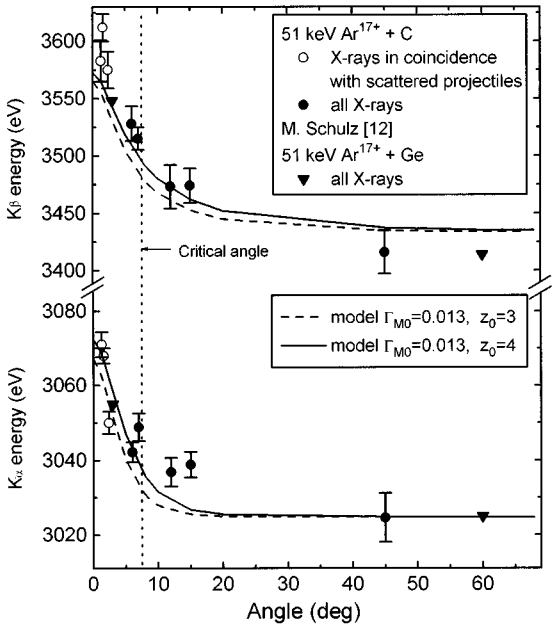

FIG. 6. $K\alpha$ and $K\beta$ x-ray transition energies from 51-keV Ar^{17+} ions incident on a graphite surface as a function of the impact angle. Theoretical curves are from the model, described in the text.

IV. MODEL FOR NEUTRALIZATION-RELAXATION OF AR^{17+} IONS

To explain our experimental findings we present a simple model which unifies the neutralization-relaxation mechanism at the surface and inside the bulk (the comparison presented in Fig. 4 strongly favors such an approach). The model describes both grazing-angle collisions and large impact angle collisions where the ion penetrates the solid. The model is based on the properties of the *K*-shell x-ray spectra emitted by Ar^{17+} ions. The following sections describe various aspects of the model and its applications.

A. Incoming part of trajectory

An ion approaching the solid surface captures electrons into relatively high quantum levels ($n\sim30$ for Ar^{17+} ions and C target) due to resonant over-barrier neutralization. As it was pointed out in the Introduction, these electrons are removed from the ion when the ion hits the surface (peeloff process), and therefore are not responsible for the final neutralization and relaxation of the ion. Because of this reason, in our model all the high shells of argon are not considered.

B. Interaction with surface and bulk

The model assumes that the major source of electrons responsible for the final neutralization and relaxation of the ion is the direct side feeding from the carbon solid into the *M* shell of argon which is considered to be the most tightly bound argon shell which could plausibly be filled directly. Note that there is close energy matching between the *K* and *L* shells of carbon and the *M* shell of argon. We exclude the possibility of direct side feeding into the Ar *K* or *L* shells because of the gross mismatch in energy between the C binding energies and these levels. As it was discussed in the Introduction, the appropriate theoretical treatment of side feeding is unknown. This forced us to apply a very simplified description of the charge exchange rate that uses adjustable parameters. The model postulates that the *M*-shell neutralization rate is given by

$$\begin{aligned} \Gamma_M &= \Gamma_{M0} q \quad \text{(below the surface)}, \\ \Gamma_M &= \Gamma_{M0} q \, \exp(-z/z_0) \quad \text{(above the surface)}, \end{aligned} \tag{1}$$

where Γ_{M0} is a constant, z is the distance from the topmost atomic layer ($z>0$ above, $z<0$ below the surface), and q is the charge state of the ion. The model uses a side-feeding rate proportional to the ion charge state q, which is equal to the nuclear charge Z of the argon ion ($=18$) minus K, L, and M population. This choice is not motivated by any *a priori* understanding of the capture process, but takes into account the fact that the capture rate must increase with both the core charge and the number of M vacancies available. The particular choice of linear q scaling is partially motivated by the well known linear q scaling of low-energy capture cross sections [28,29]. It is interesting to note that the over-barrier model [28] gives the same q dependence.

The form of the side-feeding rate (1) is probably the most central single postulate of our model. It describes a side feeding which evolves smoothly from a constant inside the solid to an exponentially decaying rate above the surface. This

TABLE I. Transition rates for Ar ions used in the model. The states used to obtain the normalization factor are listed together with references. Notation in the third column used in Refs. [34,36]. The *defect* configuration $[1s]$ is equivalent to an electronic configuration $1s^1 2s^2 2p^6 3s^2 3p^6$ of argon.

Transition	Rate in a.u. ($=4.13\times10^{16}$ s^{-1})	State used for normalization (defect configuration)	References
KLL	$\Gamma=3.18\times10^{-4}(2-n_K)n_L(n_L-1)\Theta(n_L-2)$	$[1s]$	[36,37,41]
KLM	$\Gamma=4.97\times10^{-5}(2-n_K)n_L n_M\Theta(1-n_L)\Theta(n_M-1)$	$[1s]$	[37,41]
KMM	$\Gamma=2.55\times10^{-6}(2-n_K)n_M(n_M-1)\Theta(n_M-2)$	$[1s]$	[37,41]
LMM	$\Gamma=9.56\times10^{-5}(8-n_L)n_M(n_M-1)\Theta(n_M-2)$	$[2s]$ and $[2p]$	[9,38,41]
$K\alpha$	$\Gamma=3.04\times10^{-4}(2-n_K)n_L\Theta(n_L-1)$	$[1s]$	[39,40]
$K\beta$	$\Gamma=2.49\times10^{-5}(2-n_K)n_M\Theta(n_M-1)$	$[1s]$	[39,40]
$L\alpha$	$\Gamma=3.24\times10^{-7}(8-n_L)n_M\Theta(n_M-1)$	$[2s]$ and $[2p]$	[38,40]

smooth transition is motivated by expected smooth decay of the electron density at the surface and is supported by the final-charge-state distribution data discussed above (Fig. 4). A more sophisticated modeling of the side-feeding process based partially on the over-barrier model is given by Burgdörfer *et al.* [4]. A justification for the exponential decay of the rate above the surface is that the M-shell neutralization rate is proportional to an overlap between the M-shell orbital of argon and electron density of the bulk. At large distances this overlap can be described as an exponential function of the ion-surface distance. A similar treatment has been previously employed by several authors [30–33]. The parameter z_0 can be expressed as [33]

$$z_0=\frac{a}{2}+\langle r_M\rangle, \tag{2}$$

where a is the distance between carbon atoms in the graphite (~4 a.u.) and $\langle r_M\rangle$ is the radius of the M shell in the argon ion. The radius of the M shell of the argon ion may be approximated by a simple hydrogenic formula,

$$\langle r_M\rangle=\frac{n^2}{Z_{\rm eff}}, \tag{3}$$

where n is the main quantum number, in this case 3, and $Z_{\rm eff}$ is the screened nuclear charge of the ion. Taking $Z_{\rm eff}=17$ (initial stage of the neutralization) and $Z_{\rm eff}=8$ (K and L shells full) gives $\langle r_M\rangle\cong0.5$ a.u. and $\cong1.1$ a.u., respectively. In this work we used $z_0=3$ a.u. and $z_0=4$ a.u. Both values fit into above estimations and, as will be demonstrated, give reasonable agreement with the experiment.

It should be emphasized that the neutralization rate (1) with the parameter $z_0\sim3$–4 a.u. excludes any inner-shell processes between argon ions and carbon atoms in the solid as a dominant neutralization mechanism. Inner-shell processes accrue at relatively small impact parameters, therefore, are expected to vanish rapidly outside the surface.

C. Time evolution of electron populations

The model takes into account KLL, KLM, KMM, and LMM Auger rates and $K\alpha$, $K\beta$, and $L\alpha$ x-ray rates. Therefore, the following set of rate equations needs to be solved:

$$\begin{aligned}
\frac{dn_M}{dt}&=\Gamma_M-2\Gamma_{KMM}-2\Gamma_{LMM}-\Gamma_{KLM}-\Gamma_{K_\beta}-\Gamma_{L\alpha},\\
\frac{dn_L}{dt}&=\Gamma_{LMM}+\Gamma_{L\alpha}-2\Gamma_{KLL}-\Gamma_{KLM}-\Gamma_{K\alpha},\\
\frac{dn_K}{dt}&=\Gamma_{KLL}+\Gamma_{KLM}+\Gamma_{KMM}+\Gamma_{K\alpha}+\Gamma_{K\beta},
\end{aligned} \tag{4}$$

where n_K, n_L, and n_M are, respectively, K-, L-, and M-shell populations. Since the initial charge state of argon is 17, the initial conditions are set to $n_K=1$ and $n_L=n_M=0$.

D. Transition rates and x-ray energies

It is well known that the transition rates, both Auger and radiative, strongly depend on the specific shell and subshell population. In our model, we have decided to neglect any subshell effects and express all rates as functions of the major shell populations only. In addition, we have adopted simple scaling weight factors for initial and final shell populations developed by Larkins [34]. In the case of an initial shell with population n_i, the scaling factor is $n_i\Theta(n_i-1)$ if one electron from this shell is involved in the decay, and $n_i(n_i-1)\Theta(n_i-2)$ if two electrons are involved. The step function $\Theta(x)$ is given by

$$\Theta(x)=1 \quad \text{for } x>0 \text{ or } x=0, \quad \Theta(x)=0 \quad \text{for } x<0. \tag{5}$$

The scaling factor for the final shell population is assumed to be proportional to the number of vacancies in this shell. Such a scaling factor was previously used by Briand *et al.* [11] to account for multiple L-shell vacancies for LMM Auger rate in argon. Recently Stolterfoht *et al.* [8] and Page *et al.* [35] used the same scaling to model LMM transitions in neon. Absolute rates are obtained by normalizing to known rates for singly ionized argon from Refs. [36–41]. Rates used in the model and the sources of normalization are listed in Table I. It should be pointed out that the $L\alpha$ x-ray rate is very small and was included in the model only for completeness.

The set of equations (4) and the radiative rates $K\alpha$ and $K\beta$ allow a determination of the fluorescence yield ω from

$$\omega=\omega_\alpha+\omega_\beta=\int \Gamma_{K\alpha}dt+\int \Gamma_{K\beta}dt, \tag{6}$$

where time integrals are performed over the total collision period.

In order to simulate an x-ray spectrum, energies of $K\alpha$ and $K\beta$ lines are expressed as a function L- and M-shell populations. Based on calculated transition energies for different ionized configurations of argon, from Bhalla [36], the following approximate expressions for $K\alpha$ and $K\beta$ energies were adopted:

$$\begin{aligned} E_{K\alpha}&=3144.3-22.2n_L-4.9n_M+0.4n_Ln_M \quad \text{(eV)},\\ E_{K\beta}&=3702.4-60.7n_L-15.9n_M+1.5n_Ln_M \quad \text{(eV)}. \end{aligned} \tag{7}$$

The above expressions together with the $K\alpha,\beta$ transition rates listed in Table I allow an evaluation of the x-ray energy spectrum. This was done by obtaining the infinitesimal contributions to the spectrum [intensity from $K\alpha,\beta$ rates, energy from Eq. (7)] at any time of the collision. The sum of all contributions gives the total K-shell x-ray spectrum. The spectrum was corrected for the experimental resolution using a Gaussian as a response function of the x-ray detector. It should be noted that the continuous population numbers in the model yield a continuous spectrum, but the experimental one consists of many discrete peaks, as shown by the high-resolution experiments [10,11,13]. However, this feature of the model is acceptable for our experiment because the resolution of SiLi detector does not resolve the lines with different shell populations. The average energies for $K\alpha,\beta$ lines were calculated from

$$\overline{E_{K\alpha}}=\frac{1}{\omega_\alpha}\int E_{K\alpha}\Gamma_{K\alpha}dt, \quad \overline{E_{K\beta}}=\frac{1}{\omega_\beta}\int E_{K\beta}\Gamma_{K\beta}dt. \tag{8}$$

E. Motion of ion

The M-shell neutralization rate (1) is position dependent, and therefore the set of equations (4) must be solved simultaneously with equations for the motion of the ion. The model assumes that the ion moves in an average plane potential of the form

$$\begin{aligned} V(z)&=2\pi Z_pZ_tn_aa_s\sum_{i=1}^{3}\frac{c_i}{d_i}\exp(-zd_i/a_s)\\ &\quad [\text{above the surface } (z>0)],\\ V(z)&=V(z=0)=\text{const}\\ &\quad [\text{below the surface } (z<0)], \end{aligned} \tag{9}$$

where Z_p and Z_t are projectile and target nuclear charges, n_a is the surface density of target atoms per unit area ($n_a=0.16$ a.u.$^{-2}$ was used), and $c_i=\{0.35,0.55,0.1\}$ and $d_i=\{0.3,1.2,6\}$ are Molière parameters [1,24]. The screening length a_s is given by

$$a_s=0.888(\sqrt{Z_p}+\sqrt{Z_t})^{-2/3} \tag{10}$$

and is equal to 0.25 a.u. for the argon projectile and the carbon target. This form of the potential is often used to describe grazing-angle motion and gives a good approximation to the trajectory. Particularly, the distance of the closest approach was found to be consistent with simulations that include interactions with individuals target atoms. The assumption that the potential below the surface is uniform reflects the fact that the neutralization-relaxation of the projectile takes place shortly after the bulk preparation, where the projectile velocity is not yet reduced. We believe that the plane potential (9,10) gives simplified, nevertheless correct, motion of an ion for both grazing and penetrating collisions. The application of the planar potential when the scattering angle is close to the critical angle ($\sim 7°$) is questionable. It is clear that in this regime some of the ions penetrate the solid and the remaining ones are reflected. In this case, our simplified treatment of the ion motion may not be precise.

The ion approaching the surface gains some amount of energy due to an image charge effect. For example, Ar^{17+} ion approaching a graphite surface with a work function of ~ 4 eV gains about 64 eV of energy [1]. This energy gain occurs at relatively large distances from the surface. In fact, the acceleration is nearly complete when the ion is ~ 9 a.u. in front of the surface. Therefore it can be assumed that the image charge acceleration is completed before the surface potential (9) becomes important and before the neutralization rate (1) starts to populate the M shell. For these reasons, in the model the image charge effect was taken into account by a simple increase of the perpendicular velocity, which is equivalent to an increase in the impact angle.

We point out that the reflection of the ion in grazing impact is caused by an internuclear repulsion between the argon ion and the carbon atoms in the bulk whereas the neutralization at small distances described in Eq. (1) is caused by the overlap of two electron clouds. This means that it is impossible for the ion to be reflected from the surface without being exposed to the neutralization by the solid. This observation is applicable to any ion-solid system, and is not affected by impact velocity or impact angle.

V. NUMERICAL RESULTS

A. Determination of Γ_{M0}

The model contains one free parameter Γ_{M0}. The numerical value of Γ_{M0} was extracted from experimental data. Figure 7 presents the simulated energy of the $K\alpha$ line as a function of Γ_{M0}. The initial ion energy was chosen to be the one used in the experiment, 51 keV, and the impact angle was 45°. For such a large impact angle, the ion penetrates the solid, the time it spends at the surface is relatively short, and therefore the value of z_0 does not strongly influence the $K\alpha$ energy. In fact, two $K\alpha$ energies for two values of z_0 are practically indistinguishable and are shown as one curve. The comparison between simulated and experimental values allows a determination of $\Gamma_{M0}=0.013$ a.u., and this value was used in the model. It is interesting to ask whether this value of Γ_{M0} is reasonable. Assuming that the neutralization rate in the solid can be expressed as

$$\Gamma_M=n_C v\sigma, \quad \sigma=\pi r^2, \tag{11}$$

where n_C is the density of carbon atoms in graphite ($=0.017$

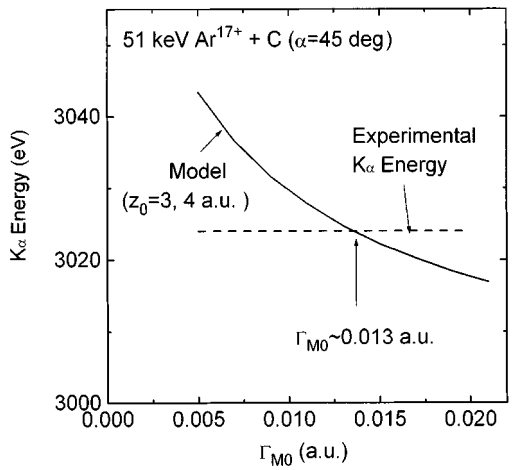

FIG. 7. $K\alpha$ transition energy predicted by the model for 51-keV Ar^{17+} ions incident on a graphite surface at 45° plotted as a function of Γ_{M0}. The model prediction matches the experimental value for $\Gamma_{M0}=0.013$ a.u.

a.u.$^{-3}$), v is the beam velocity, and σ is the cross section for the charge exchange, one can estimate the value of a geometrical capture radius r. Using $\Gamma_{M0}=0.013$ a.u. and $q\sim10$ the capture radius turns out to be ~3 a.u. This value seems reasonable for the capture inside the solid.

B. Incidence-angle dependence of $K\alpha$, $K\beta$ energies and total fluorescence yield

The simulations for the angular dependence of the average $K\alpha$ and $K\beta$ energies agree well with the experimental data shown in Fig. 6. The shape of the dependence and the absolute value of both energies reproduce the experimental data well. The simulation correctly predicts relatively small energy changes for angles below $\sim7°$, i.e., for penetrating collisions. On the other hand, grazing-angle impact causes a much stronger upwards shift for both lines. Comparing two values of z_0 used in simulation, $z_0=4$ a.u. seems to work better. The energies rise at small impact angles because the ion approaching the surface at a small angle is only slowly neutralized by rate (1). This means the average L and M population at the time of x-ray emission is lower, compared to normal incidence, and the energies of both x-ray lines are shifted upwards.

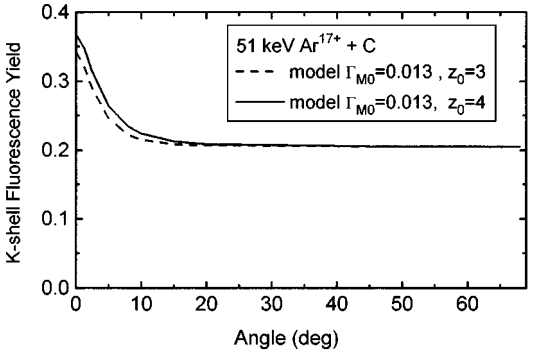

FIG. 8. Total fluorescence yield predicted by the model for K-shell x-ray transitions for 51-keV Ar^{17+} ions incident on a graphite surface as a function of the impact angle.

The total K-shell fluorescence yield as a function of the impact angle is shown in Fig. 8. For the angles above the critical angle the fluorescence yield is almost constant, but at small angles significantly increases. The model predicts 40–50 % enhancement of the fluorescence yield for small angles, comparing to normal incidence. This is consistent with the approximately 30% increase of the fluorescence yield for 3° impact, compared to 60° impact reported by Schultz *et al.* [12].

The x-ray spectrum obtained from the model is presented in Fig. 5. The theoretical curve was normalized to fit the height of the experimental $K\alpha$ peak. The theoretical spectrum was corrected for the experimental resolution of 220 eV, which was obtained experimentally using the $K\alpha$ fluorescence emission from chlorine. It can be seen that the model correctly describes the relative intensities of $K\alpha$ and $K\beta$ lines, as well as the widths of both peaks.

C. Time evolution of shell populations

The time evolution of K-, L-, and M-shell populations calculated from the model for normal incidence and grazing-angle incidence are shown in Figs. 9 and 10, respectively. For clarity, the penetration depth and the ion-surface distance are indicated. The L- and M-shell populations during the x-ray emission are significantly different in two scattering regimes. In normal incidence about five electrons from the L shell and eight electrons from the M shell are present at the time the K shell is filled. For grazing-angle scattering these populations are reduced to about three L electrons and five M electrons. In the case of normal incidence the whole neutralization-relaxation takes place in the solid. For grazing-angle collision the K shell is filled before the ion reaches the distance of the closest approach. The filling of the L shell takes longer, but is completed during the duration of the collision. The final charge state of the ion is ~0.1, which agrees with experimentally observed (Fig. 2) almost full neutralization of Ar^{17+} ions at this velocity. The relatively short time for the K-shell filling suggests that the introduction of a second K-shell vacancy, as would be the case for Ar^{18+} ions, would not change the outcome of the grazing collision, i.e., the ion will be fully neutralized. Finally, it is clear that the relaxation of lower charge states will be also completed due to a smaller number of initial vacancies.

VI. CONCLUSIONS

We have observed that argon ions at velocities between 0.15 and 0.62 a.u. in different incidence charge states experience almost full charge-state equilibration during grazing-angle collisions with a graphite surface. The number of inner-shell vacancies carried by the projectile has only a minor effect on the final charge state which can be noticed for charge states of $q=2$ and larger. The average charge state is almost unaffected by the inner-shell vacancies and this trend is present for impact velocities up to 0.62 a.u. The velocity dependences of the average charge state following a grazing-angle scattering and following penetration through a thin carbon foil show a strong similarity. These findings indicate that neutralization mechanisms in grazing-angle collisions and during the penetration of the bulk are similar.

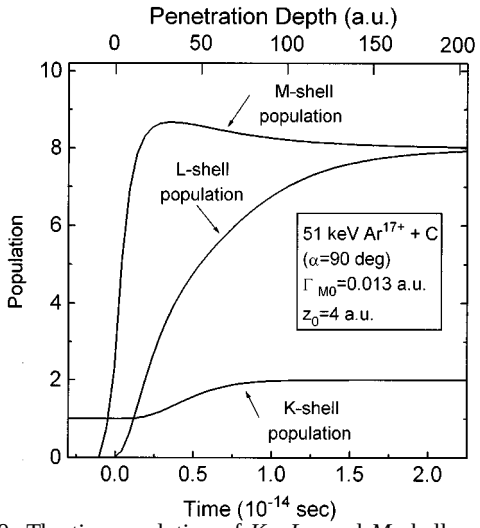

FIG. 9. The time evolution of K-, L-, and M-shell populations for 51-keV Ar^{17+} and 90° impact angle, as predicted by the model described in the text. The penetration depth in the solid is shown for comparison.

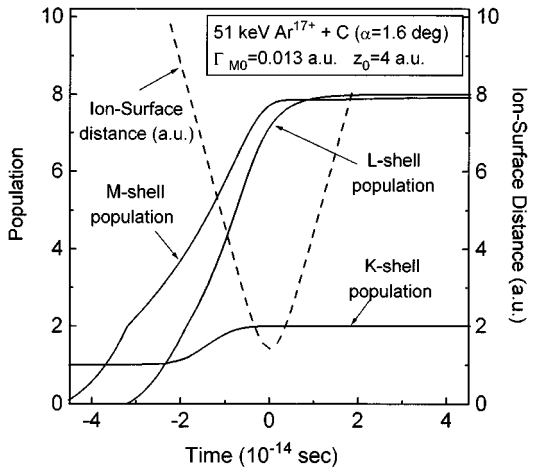

FIG. 10. The time evolution of K-, L-, and M-shell populations for 51-keV Ar^{17+} and 1.6° impact angle as predicted by the model described in the text. The ion-surface distance is shown for comparison.

We have presented a side-feeding model which, together with pure atomic relaxation rates, is capable of explaining the basic features of x-ray emission by Ar^{17+} projectiles for different impact angles. The filling of inner-shell vacancies is not via decay cascades from highly excited states but via side feeding that occurs at a short distance above the surface. The side feeding is not into deeply bound shells which carry most of the projectile potential energy but into an intermediate shell (M shell for argon). Since no close energy-level matching is required, this is likely to be similar for any target surface. The neutralization of the ion in a grazing-angle collision is inevitable, since the reflection of the ion and the neutralization of the ion both require penetration of the electron cloud of the surface. The atomic transitions (Auger and radiative) from intermediate shells are sufficient to allow the complete filling of inner shells and the dissipation of the potential energy initially carried by the ion. The postulate that the side feeding inside the solid does not terminate at the surface, but extends beyond the surface, successfully describes both the rapid neutralization of the ion and the inner-shell x-ray emission during grazing-angle collisions. The relatively slow decay of the neutralization rate outside the solid ($z_0 \sim 3-4$ a.u.) rules out any inner-shell processes as a dominant side-feeding mechanism near the surface, and points at the electron gas density as the cause of the neutralization.

Our experimental data and the success of our model show a substantial similarity between the neutralization in front of the surface and neutralization inside a solid foil. This fact stresses a need for a model which applies to both regimes.

ACKNOWLEDGMENTS

We thank Dr. I. Lagadic for carrying out atomic force microscope studies of the graphite surface. This work was supported by the Division of Chemical Sciences, Office of Basic Energy Sciences, Office of Energy Research, U.S. Department of Energy.

[1] J. Burgdörfer, in *Review of Fundamental Processes and Applications of Atoms and Ions*, edited by C. D. Lin (World Scientific, Singapore, 1993).

[2] F. W. Meyer, L. Folkerts, and S. Schippers, Nucl. Instrum. Methods, Phys. Res. Sect. B **100**, 366 (1995).

[3] L. Folkerts, S. Schippers, D. M. Zehner, and F. W. Meyer, Phys. Rev. Lett. **74**, 2204 (1995).

[4] J. Burgdörfer, C. Reinhold, and F. W. Meyer, Nucl. Instrum. Methods Phys. Res. Sect. B **98**, 415 (1995).

[5] J. Burgdörfer, P. Lerner, and F. W. Meyer, Phys. Rev. A **44**, 5674 (1991).

[6] H. Kurz, K. Toglhoffer, H. P. Winter, F. Aumayr, and R. Mann, Phys. Rev. Lett. **69**, 1140 (1992).

[7] H. J. Andrä, A. Simionovici, T. Lamy, A. Brenac, G. Lamboley, J. J. Bonnet, A. Fleury, M. Bonnefoy, M. Chassevent, S. Andriamonje, and A. Pesnelle, Z. Phys. D **21**, 135 (1991).

[8] N. Stolterfoht, A. Arnau, M. Grether, R. Köhrbrück, A. Spieler, R. Page, A. Saal, J. Thomaschewski, and J. Bleck-Neuhaus, Phys. Rev. A **52**, 445 (1995).

[9] E. D. Donets, Nucl. Instum. Methods Phys. Res. Sect. B **9**, 522 (1985).

[10] J. P. Briand, L. de Billy, P. Charles, S. Essabaa, P. Briand, J. P. Desclaux, R. Geller, S. Bliman, and C. Ristori, Phys. Rev. Lett. **65**, 159 (1990).

[11] J. P. Briand, L. de Billy, P. Charles, S. Essabaa, P. Briand, R. Geller, J. P. Desclaux, S. Bliman, and C. Ristori, Phys. Rev. A **43**, 565 (1991).

[12] M. Schulz, C. L. Cocke, S. Hagmann, M. P. Stöckli, and H. Schmidt-Bocking, Phys. Rev. A **44**, 1653 (1991).

[13] B. d'Etat, J. P. Briand, G. Ban, L. de Billy, J. P. Desclaux, and P. Briand, Phys. Rev. A **48**, 1098 (1993).

[14] J. P. Briand, S. Bardin, D. H. Schneider, H. Khemliche, J. Jin, and M. Prior (unpublished).

[15] M. P. Stöckli, C. L. Cocke, and P. Richard, Rev. Sci. Instrum. **61**, 242 (1990).
[16] M. P. Stöckle, R. M. Ali, C. L. Cocke, M. L. A. Raphaelian, P. Richard, and T. N. Tipping, Rev. Sci. Instrum. **63**, 2822 (1992).
[17] N. J. Wu, and A. Ignatiev, Phys. Rev. B **25**, 2983 (1982).
[18] A. M. Baro, R. Miranda, J. Alaman, N. Garcia, G. Binning, H. Rohrer, Ch. Gerber, and J. L. Carroscosa, Nature **315**, 253 (1985).
[19] G. Binnig, H. Fuchs, Ch. Gerber, H. Rohrer, E. Stoll, and E. Tosatti, Europhys. Lett. **1**, 31 (1986).
[20] J. Schneir, R. Sonnenfeld, P. K. Hansma, and J. Tersoff, Phys. Rev. B **34**, 4979 (1986).
[21] I. L. Spain, *Chemistry and Physics of Carbon*, edited by P. L. Walker and P. A. Thrower (Dekker, New York, 1981), Vol. 16.
[22] G. Binnig, H. Fuchs, Ch. Gerber, H. Rohrer, E. Stoll and E. Tosatti, Europhys. Lett. **1**, 31 (1986).
[23] F. Stölze, and R. Pfandzelter, Surf. Sci. **251/252**, 383 (1991).
[24] R. Pfandzelter, and F. Stölze, Nucl. Instrum. Methods Phys. Res. Sec. B **72**, 163 (1992).
[25] H. W. M. Salemink, I. P. Batra, H. Rohrer, E. Stoll, and E. Weibel, Surf. Sci. **181**, 139 (1987).
[26] Hans D. Betz, in *Methods of Experimental Physics*, edited by P. Richard (Academic, London, 1980), Vol. 17.
[27] K. Shima, T. Mikumo, and H. Tawara, At. Data Nucl. Data Tables **34**, 357 (1986).
[28] N. Bohr, and J. Linhard, K. Danske Vidensk. Selsk. Mat.-Fys. Meddr. **28**, No. 7 (1954).
[29] H. Ryufuku, K. Saski, and T. Watanabe, Phys. Rev. A **14**, 579 (1976).
[30] H. D. Hagstrum, Phys. Rev. **104**, 672 (1956).
[31] H. D. Hagstrum, in *Inelastic Ion-Surface Collisions*, edited by N. H. Tolk, J. C. Tully, W. Heiland, and C. W. White (Academic, New York, 1977).
[32] J. Bardeen, Phys. Rev. Lett. **6**, 57 (1961).
[33] H. Winter, and R. Zimny, in *Coherence in Atomic Collision Physics*, edited by J. Beyer, K. Blum, and R. Hippler (Plenum, London, 1988).
[34] F. P. Larkins, J. Phys. B **9**, L29 (1971).
[35] R. Page, A. Saal, J. Thomaschewski, L. Aberle, J. Bleck-Neuhaus, R. Köhrbrück, M. Grether, and N. Stolterfolht, Phys. Rev. A **52**, 1344 (1995).
[36] C. P. Bhalla, Phys. Rev. A **8**, 2877 (1973).
[37] E. J. McGuire, Phys. Rev. A **2**, 273 (1970).
[38] E. J. McGuire, Phys. Rev. A **3**, 587 (1971).
[39] S. T. Manson, and D. J. Kennedy, At. Data Nucl. Data Tables **14**, 111 (1974).
[40] J. H. Scofield, At. Data Nucl. Data Tables **14**, 121 (1974).
[41] M. H. Chen, B. Crasemann, and H. Mark, At. Data Nucl. Data Tables **24**, 13 (1979).